Journal of Rock Mechanics and Geotechnical Engineering 13 (2021) 643–652

Contents lists available at ScienceDirect

Journal of Rock Mechanics and Geotechnical Engineering

journal homepage: www.jrmge.cn

Full Length Article

Engineering and microstructure properties of contaminated marine sediments solidified by high content of incinerated sewage sludge ash

Jiang-Shan Li [a,b,c], Yifan Zhou [d], Xin Chen [a,b], Qiming Wang [d], Qiang Xue [a,c,*], Daniel C.W. Tsang [d], Chi Sun Poon [b,d,**]

[a] State Key Laboratory of Geomechanics and Geotechnical Engineering, Institute of Rock and Soil Mechanics, Chinese Academy of Sciences, Wuhan, 430071, China
[b] IRSM-CAS/HK PolyU Joint Laboratory on Solid Waste Science, Hung Hom, Kowloon, Hong Kong, China
[c] Hubei Province Key Laboratory of Contaminated Sludge and Soil Science and Engineering, Wuhan, 430071, China
[d] Department of Civil and Environmental Engineering, The Hong Kong Polytechnic University, Hung Hom, Kowloon, Hong Kong, China

ARTICLE INFO

Article history:
Received 29 June 2020
Received in revised form
24 September 2020
Accepted 25 October 2020
Available online 9 December 2020

Keywords:
Contaminated marine sediment (CMS)
Incinerated sewage sludge ash (ISSA)
Solidification/stabilization (S/S)
Heavy metals
Construction material

ABSTRACT

Management of incinerated sewage sludge ash (ISSA) and dredged contaminated marine sediments (CMSs) is a great challenge for Hong Kong and other coastal cities due to limited landfilling capacity. The present study investigates the use of high content (20% of sediment by mass) of ISSA in combination with cement/lime for solidification/stabilization (S/S) treatment of CMSs to provide a way to reuse the wastes as construction materials. The results showed that ISSA being a porous material was able to absorb a large amount of water rendering a more efficient solidification process of the marine sediment which normally had a very high water content (~80%). The S/S treatment improved the engineering properties of the sediment, but reduced the workability, especially for the lime-treated samples. Lime can be used to replace ordinary Portland cement (OPC) for better heavy metal immobilization and carbon emission reduction. The hardened sediment samples prepared with 10% of lime and 20% of ISSA could attain a strength of 1.6 MPa after 28 d of curing. In addition, leaching tests confirmed that there was no environmental risk induced by these stabilized materials. The formation of hydrated cementitious compounds including calcium silicate hydrate (C–S–H)/calcium aluminate silicate hydrate (C-A-S-H)/hydrocalumite/calcite was mainly responsible for the strength development in the ISSA/lime-treated sediments.

1. Introduction

Safe treatment and resource recycling of the alarmingly increasing amount of solid wastes have presented significant financial and environmental burdens to municipalities. Meanwhile, several hundred millions of tons of contaminated sediments are dredged annually from harbors around the world (Lirer et al., 2017). Hong Kong has the largest sewage sludge incinerator (T·Park) in the world and it is important that the incinerated sewage sludge ash (ISSA) produced is managed in the best possible way for sustainable development (Li et al., 2017a). A large volume of soft sediment with high water content at a marine site may be too weak to support the civil engineering structure (e.g. bridge piers or runway). Although extensive studies on the possible ISSA recycling had been carried out, practical applications of the developed technologies are still scare, mostly due to its relatively low pozzolanic activity for strength development in construction materials and the high cost to recovery of phosphorus (Chen and Poon, 2017; Fang et al., 2018). However, studies confirm that ISSA/cement has potential applications in the field of geotechnical engineering (Li et al., 2019). ISSA/cement in a fixed ratio of 4:1 could be used as a stabilizer to improve the strength of soft, cohesive, subgrade soil, when the maximum additional amount of the admixture was set as 16% (Chen and Lin, 2009). Previous studies (e.g. Li et al., 2017a; Chen et al., 2018) also showed the feasibility of using a small amount of ISSA (<20%) as a cement replacement for producing concrete blocks or cement mortars. However, to the best of authors' knowledge, studies on the effects of utilizing high content of ISSA

* Corresponding author.
** Corresponding author.
E-mail addresses: qxue@whrsm.ac.cn (Q. Xue), cecspoon@polyu.edu.hk (C.S. Poon).

Peer review under responsibility of Institute of Rock and Soil Mechanics, Chinese Academy of Sciences.

https://doi.org/10.1016/j.jrmge.2020.10.002

(e.g. >20%) as a supplementary cementitious material (SCM) in producing construction materials are rarely reported.

In 2014, about 29 Mm^3 contaminated marine sediments (CMSs) were dredged in Hong Kong (Wang et al., 2015a). The ISSA presents high adsorption capacity to water and some heavy metals and thus has the potential to be used as an SCM in treating heavy metals contaminated sediment (Li and Poon, 2017). Thus, the CMS needs improvements to provide the required strengths. In the last decade, the lime or ordinary Portland cement (OPC) treated sediments were usually used in sub-base/roadbase layers and filling construction (Wang et al., 2015b). Nowadays, increasingly amounts of SCMs (e.g. pulverized fly ash (PFA) and ground-granulated blast-furnace slag (GGBS)) are being used as cement replacements (Garcia-Lodeiro et al., 2013; Zentar et al., 2012; Wang et al., 2015a, 2018). Therefore, it is deduced that lime may be used to replace traditional OPC and be mixed with ISSA for solidification/stabilization (S/S) treatment of soft CMS. But the mechanisms controlling strength development and heavy metal immobilization in the CMS S/S treated by ISSA/lime are still unclear.

This study attempts to explore the S/S mechanisms after mixing the CMS with high content of ISSA to produce a sub-base or filling material. The influences of binder contents and curing time on strength, deformation, durability, heavy metal leaching, and microstructure development were investigated. Several tests were conducted on the S/S-treated sediment, including natural dewatering, unconfined compressive strength (UCS), toxicity characteristic leaching procedure (TCLP), dynamic tank leaching, X-ray diffraction (XRD), scanning electron microscopy with energy dispersive X-ray spectroscopy (SEM-EDX) and mercury intrusion porosimetry (MIP).

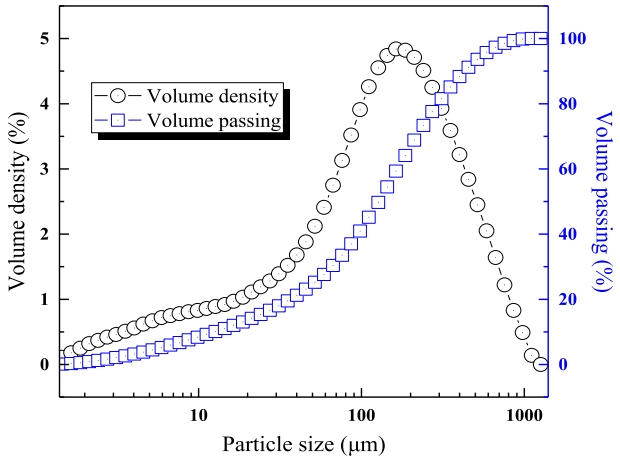

Fig. 1. Particle size distributions of dredged sediment.

Table 2
Design of sediment mixtures (mass ratio).

Symbol	Cement	Lime	Sludge ash (ISSA)	Sediment
SD			0.2	1
C5	0.05		0.2	1
C10	0.1		0.2	1
L5		0.05	0.2	1
L10		0.1	0.2	1

Note: SD denotes sediment treated without cement/lime; C(5/10) denotes sediment treated with cement under the dosage of 5 or 10; L(5/10) denotes sediment treated with lime under the dosage of 5 or 10.

2. Materials and methods

2.1. Binder materials and sediments

In this study, the binder materials included OPC equivalent to ASTM Type 1 cement and industrial grade quicklime with 65% CaO produced in Hong Kong. The ISSA from T·Park was directly collected and the characteristics of ISSA had been reported in our previous work (Li et al., 2017b). The ISSA was oven-dried at 105 °C before use.

The marine sediment used was dredged from a nearshore location in Hong Kong waters and it was sieved through 4.75 mm sieve to obtain homogenous fine particle portion for the experiment. A laser diffraction particle size analyzer was used to analyze particle size distribution (PSD) of the fine portion (<2000 μm) of the sediment sample, as shown in Fig. 1. The sediment consisted of 0.34% clay, 16.69% silt, 38.33% gravel, and 44.64% sand fractions. The total heavy metal concentrations along with physico-chemical properties of sediment are summarized in Table 1.

2.2. S/S sample preparation

The sediment mortar samples were prepared with various binder ratios by OPC/lime and ISSA according to the mix design listed in Table 2.

The marine sediments with 77.71% of water content were mixed with the binder for 3 min in a standard mechanical drum type mixer to produce uniform mixtures. Afterwards, the fresh mixtures were cast into ϕ50 mm × 50 mm plastic cylindrical mold and vibrated for 1 min to eliminate entrapped air bubbles. All the samples were wrapped with polyethylene sheets to avoid water loss and kept at (23 ± 2) °C with relative humidity of 95%. After curing for the preset time, the samples were demolded for the tests.

Table 1
Physico-chemical properties of dredged sediment.

Property		Value	Method
Heavy metal concentration	Cu	74.04 mg/kg	Inductively coupled plasma atomic emission spectrometry (ICP-AES) (SPECTROBLUE)
	Zn	154.72 mg/kg	
	Pb	73.58 mg/kg	
	Cr	37.3 mg/kg	
	Ni	16.22 mg/kg	
	As	34.08 mg/kg	
	Cd	2.18 mg/kg	
Contamination level		Medium (category M)	HK EWTB (2002)
Water content		77.71%	Oven-dried at 105°C
Salinity		24.8 g/kg	Conductivity meter (WTW inoLab Cond 720)
Organic matter content		4.2%	Loss on ignition at 550 °C
Specific gravity		2.49	Water pycnometer method
pH value		8.51	1:10 dry sample: deionized water
Main chemical compositions		SiO_2 (58.05%), Al_2O_3 (21.99%)	X-ray fluorescence (XRF) (Rigaku Supermini200)

2.3. Test methods

2.3.1. Natural dewatering

The top part of cylindrical molds after sample casting was uncovered and in contact with air at room temperature of (23 ± 2) °C with the controlled relative humidity (50%). The mass of each sample was regularly measured at 3 d, 7 d, 14 d and 28 d during natural dewatering process to calculate water content at each time.

2.3.2. Workability

The workability of the fresh sediment mortar mixtures was tested following the flow table spread (FTS) method (ASTM C1437-15, 2015).

2.3.3. Compressive strength

A universal testing machine (Testometric CXM 500-50 KN) was employed to determine the compressive strength after 7 d, 28 d and 90 d of curing and the loading rate was 0.3 mm/min according to BS EN12390-3(2009). The averages of the duplicates and the loading-displacement figures were recorded. The failure strains and deformation modulus E_{50} can therefore be computed.

2.3.4. Durability (water soaking)

To test the durability of sediment mortar samples, they were stored in a distilled water tank for 30 d after being cured for 28 d and the strength after soaking was determined and compared with the strength cured for 28 d.

2.3.5. Heavy metal leachability

Two leaching tests were conducted to investigate the potential leachability of heavy metals from the sediment mixtures as follows. The concentrations of heavy metals in the leachate separated by filtration with a 0.45 μm mixed cellulose esters membrane filter were measured by ICP-AES (SPECTROBLUE) after concentrated nitric acid digestion in a digestion block.

(1) According to US EPA (1992) method 1311, the toxicity characteristic leaching procedure (TCLP) was recognized to determine the suitability of landfilling material. The sediment mortar samples were leached with 0.1 mol/L acetic acid (pH value of 2.88) at a liquid-to-solid ratio of 20 L/kg. The samples together with the proportioned leachate were placed in capped polypropylene bottles and rotated for 18 h at 30 revolutions per minute (rpm).

(2) Semi-dynamic leaching test was conducted on the sediment mortars that were immersed in 1 L deionized water. The test lasted for 11 d at (23 ± 2) °C and the deionized water was renewed and 10 mL of the leachate was collected after 2 h, 7 h and 24 h during the first day, and daily extraction was carried out for the rest 10 d (Li et al., 2019).

According to Eq. (1), the cumulative fraction leached (CFL) of heavy metals can be calculated. The diffusion coefficient (*De*) of heavy metals was calculated using Eq. (2).

$$CFL = \frac{A_t}{A_0} = \frac{1}{A_0}\Sigma_i(c_i V_{L,i}) \tag{1}$$

$$D_e = \frac{\pi}{4}\left(\frac{V}{S}\right)^2 \frac{CFL^2}{t} \tag{2}$$

where A_t is the cumulative mass of the heavy metals leached from the medium surface (mg); A_0 is the total mass of substance contained in the samples prior to the test (mg); c_i is the measured concentration of the leached heavy metals in the leachate at I th test interval (mg/L); $V_{L,i}$ is the volume of leachate (L); V is the volume of specimen (cm^3); S is the surface of the sample used in the test (cm^2); and t is the leaching time (s).

2.3.6. Microscopic investigations

For the microscopic tests, after the specified curing period, the sediment mortar samples were immersed in ethanol for 7 d to arrest hydration and then placed in a vacuum oven at 60 °C to remove ethanol and prevent carbonation. The crystalline phases of ball milled specimens were detected by an XRD (Rigaku SmartLab) with CuKα radiation, scanning from $2\theta = 5°–60°$. The step size was 0.02° and the operation conditions were 40 kV and 30 mA.

A SEM-EDX (Tescan Vega 3) under accelerating voltage of 20 kV was used to analyze surface morphologies of gold-coated fractured specimens of the sediment mortar samples. The pore structure of the sediment mortars was tested by the MIP test (Micromeritics Autopore IV 9500 Series). The specimens for MIP were prepared by breaking the mortar samples into small pieces between 2.36 mm and 5 mm. The measured pore size ranged from 7 nm to 150 μm under a maximum intrusion pressure of 207 MPa.

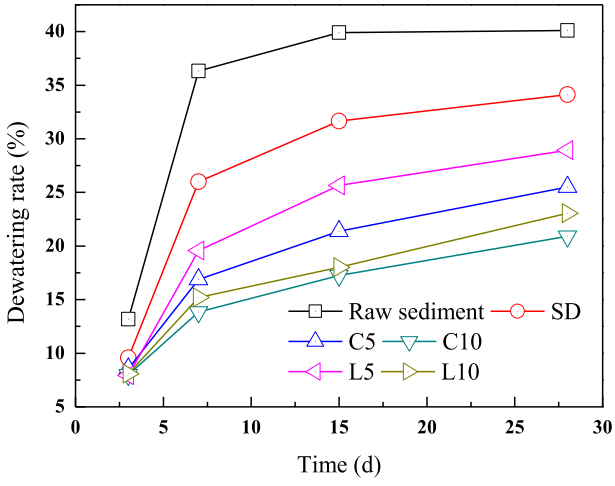

Fig. 2. Natural dewatering of solidified sediments.

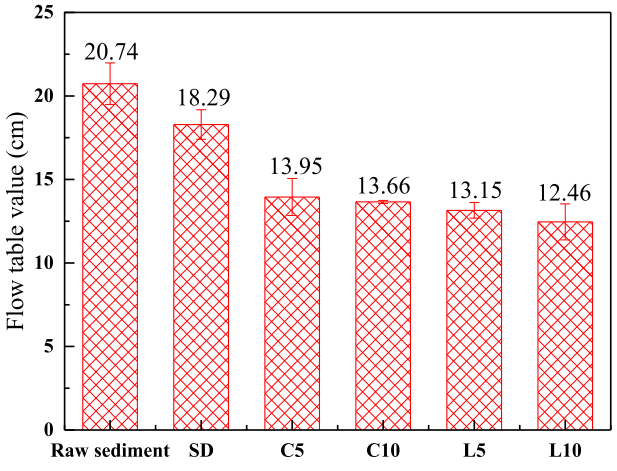

Fig. 3. Flow table spread values of the fresh sediment mortars.

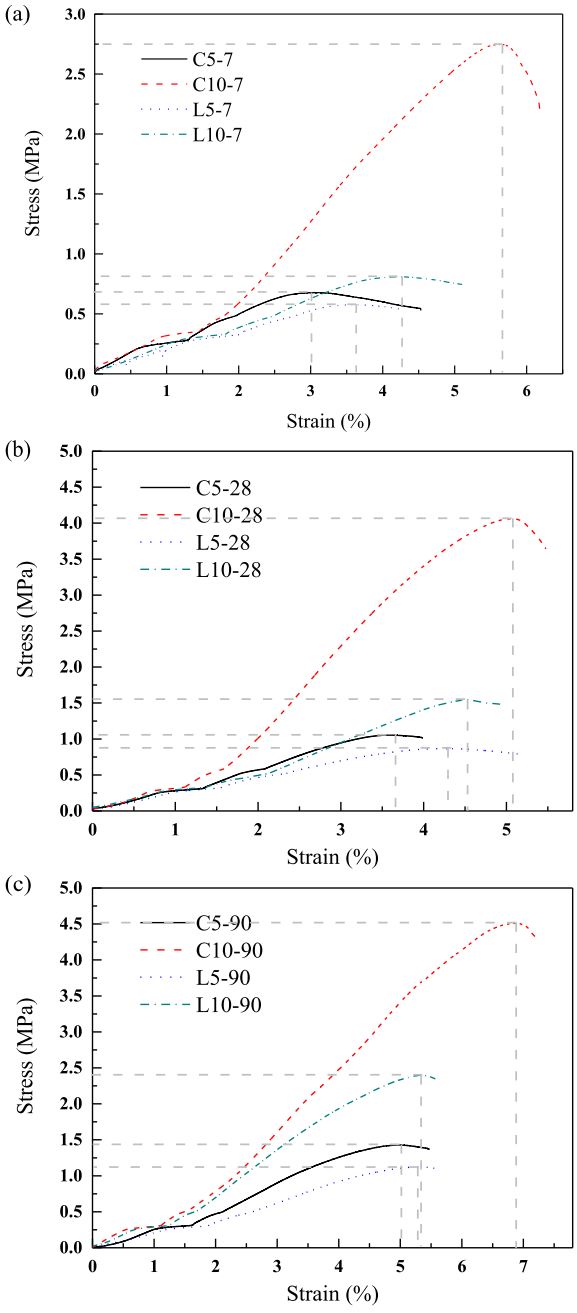

Fig. 4. Stress–strain curves of mortar samples at (a) 7 d, (b) 28 d and (c) 90 d of curing.

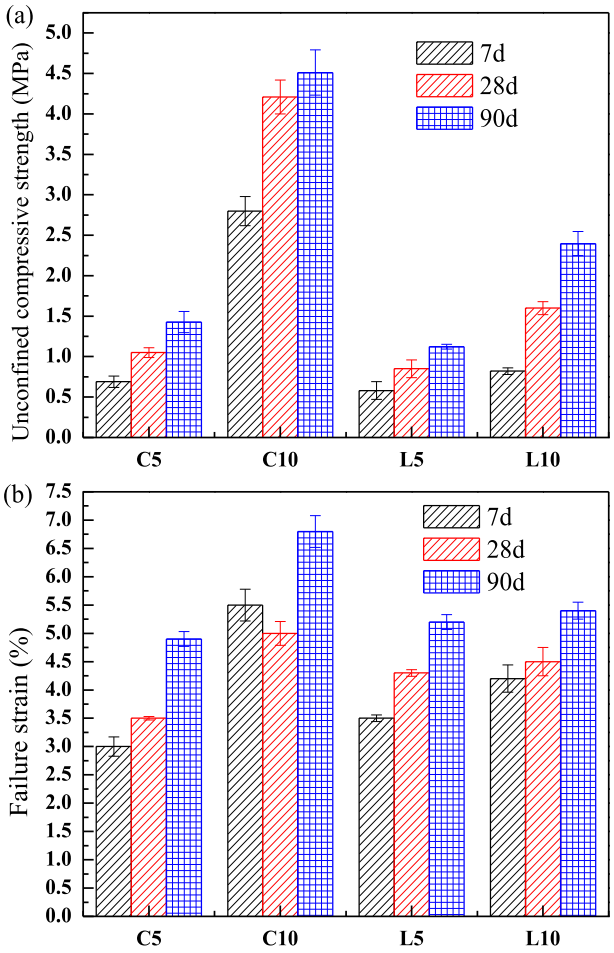

Fig. 5. (a) Compressive strength and (b) Failure strain of mortars at 7 d, 28 d and 90 d.

3. Results and discussion

3.1. Natural dewatering

Water evaporated from the sediment mortar samples may lead to size and volume shrinkage. For the purpose of use as construction materials, a small volume decrease of the mortar samples was desirable to ensure structural stability (Zentar et al., 2011). Fig. 2 depicts the change of natural dewatering rate of the sediment mortar samples with elapsed time. All the mortar samples showed an increasing trend of dewatering rate and the rate increased remarkably from approximately 13% at day 3–36% at day 7, and almost remained steady from 14 d. The raw sediment had the highest dewatering rate due to its high-water content. With addition of ISSA, it is clear that the dewatering rate decreased significantly, which was attributed to pores and irregular morphology of ISSA particles and its high-water adsorption capacity. After blended with OPC or lime, reduction in dewatering rate occurred, while further increasing the OPC or lime contents caused a slight decrease of the dewatering rate. This might be related to the fact that the binder materials had consumed a portion of the water in the pozzolanic reactions (Wang et al., 2017). Compared with lime, the cement sample had a lower dewatering rate most likely due to the higher water consumption of cement hydration and the denser structure of the cement incorporated samples.

3.2. Workability

The FTS values of the fresh sediment mortar samples are shown in Fig. 3. The flow of SD samples was lower than that of the raw sediment after incorporation of ISSA as the ISSA particles absorbed a large amount of water from the sediment. The flowability dropped further after using OPC and lime, and the mortars with OPC (C5 and C10) had slightly higher FTS values than lime, suggesting their lower viscosity. This may be attributed to a higher capability of lime to absorb and retain water, which thickened the mixtures because of enhanced cohesivity (Senff et al., 2010; Izaguirre et al., 2010). Although there was reduction in the workability of the sediment mortars, the flowability was still suitable for construction processes (ASTM C 109, 2008).

3.3. Compressive strength and engineering properties of mortars

The stress–strain relationships of C5, C10, L5 and L10 samples at all the curing ages are plotted in Fig. 4. The peak stress increased significantly from 7 d to 90 d and C10 had the highest peak stress among all the samples, followed by L10 regardless of curing age. All the sediment mortar samples experienced deformation first, and then the strength of C10 increased linearly until reaching the peak stress (Fig. 4a and b), while the other samples showed a nonlinear and slow stress increase due to plastic deformation. After reaching the peak stress, the stress started to reduce with increase of strain for all the samples. It is clear that C10 was more brittle than the other samples. At the later age (Fig. 4c), all the samples showed a linear increase of stress following the initial deformation. C5 and L5 then experienced some plastic deformation, while C10 and L10 showed linear increase of stress. After reaching the peak stress, the stress of C5 and L5 decreased slightly as they were less stiff than C10 and L10.

The parameters including UCS, failure strain, and deformation modulus E_{50} can be calculated from the full stress–strain curves. The peak stress is the UCS, the strain at the peak stress is considered as the failure strain, and the deformation modulus in this study is defined as the secant modulus at 50% of UCS. The UCS and failure strain of the mortar samples at 7 d, 28 d and 90 d are presented in Fig. 5a and b, respectively. As the raw sediment and the SD samples did not have sufficient strength upon demolding, they cannot be compared directly in the figures. As shown in Fig. 5a, the strength of all the mortars increased with increasing curing time and binder contents. However, only C10 and L10 samples at 28 d met the strength criteria of 1.15 MPa at 28 d (ACI, 1999) to be used as low strength filling materials. The sediment treated by lime-ISSA also could provide sufficient strength, even though they had a lower strength value than OPC-ISSA treated sediment. This can be attributed to the larger amount of C–S–H gel formed during OPC hydration. The C10 sample had the highest strength among all the mortar samples and its 28-d strength reached 4.21 MPa, which met

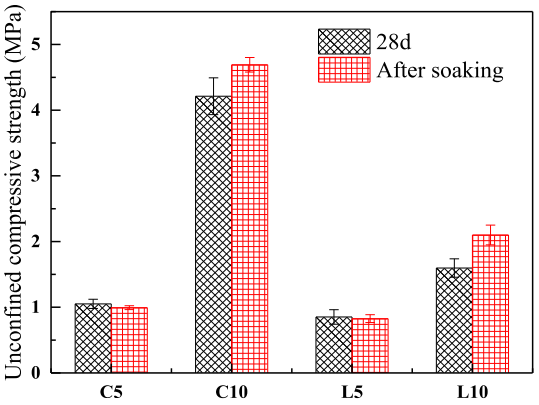

Fig. 7. Strength of mortar samples at 28 d of curing and after further soaking for 30 d.

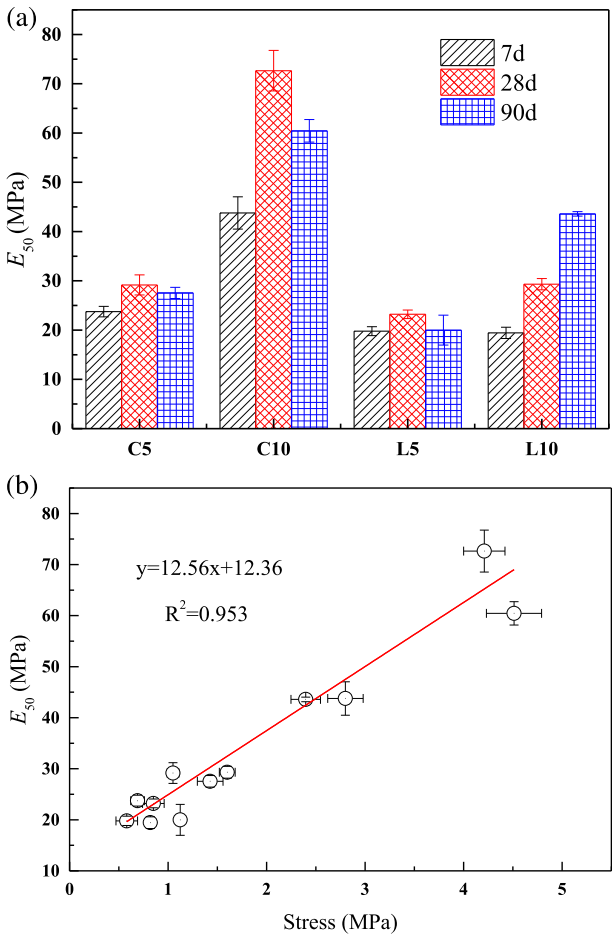

Fig. 6. (a) Deformation modulus E_{50} and (b) Relationship between E_{50} and stress.

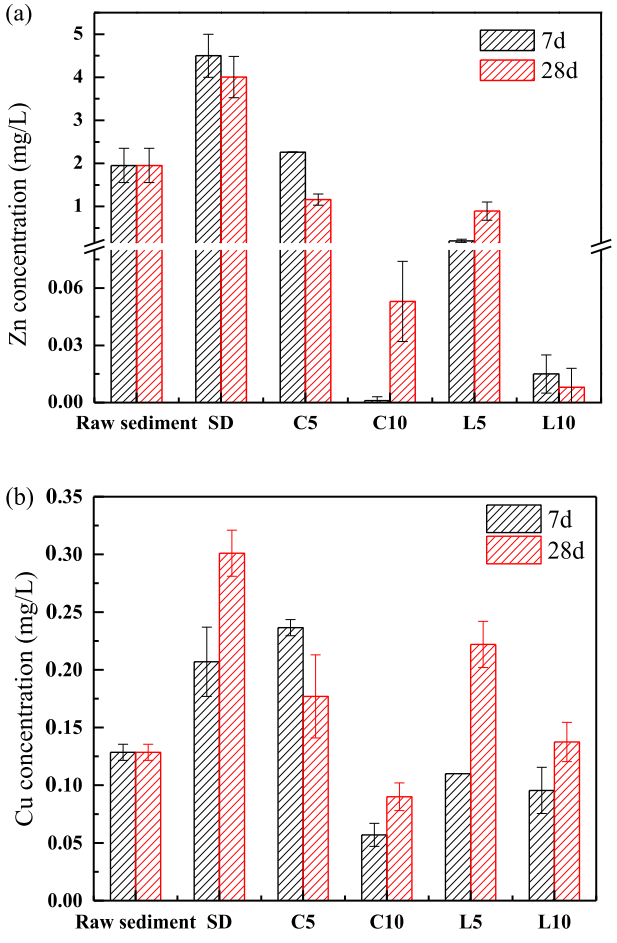

Fig. 8. (a) Zn and (b) Cu TCLP leachate concentrations.

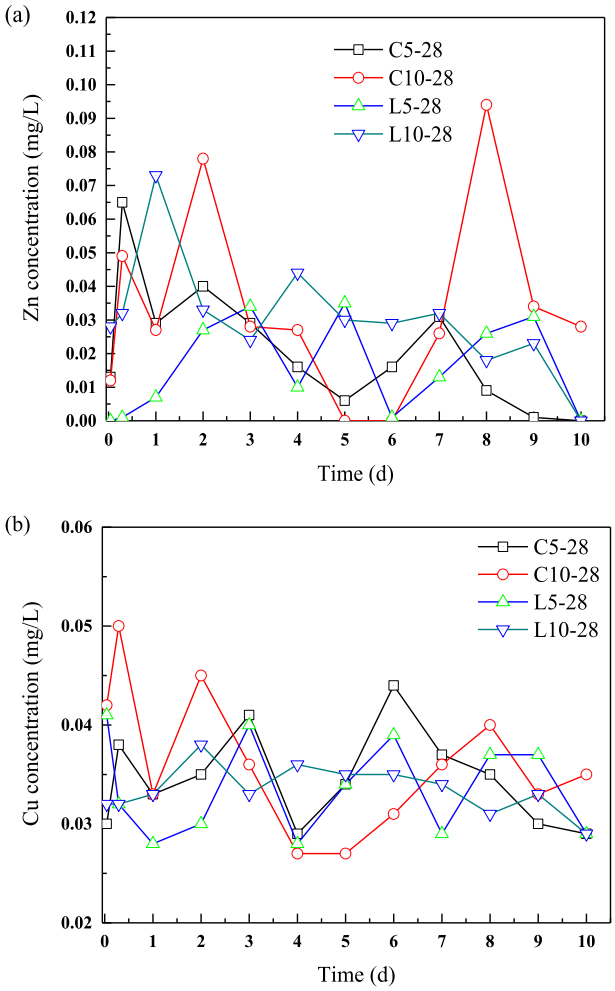

Fig. 9. Concentrations of (a) Zn and (b) Cu from semi-dynamic leaching.

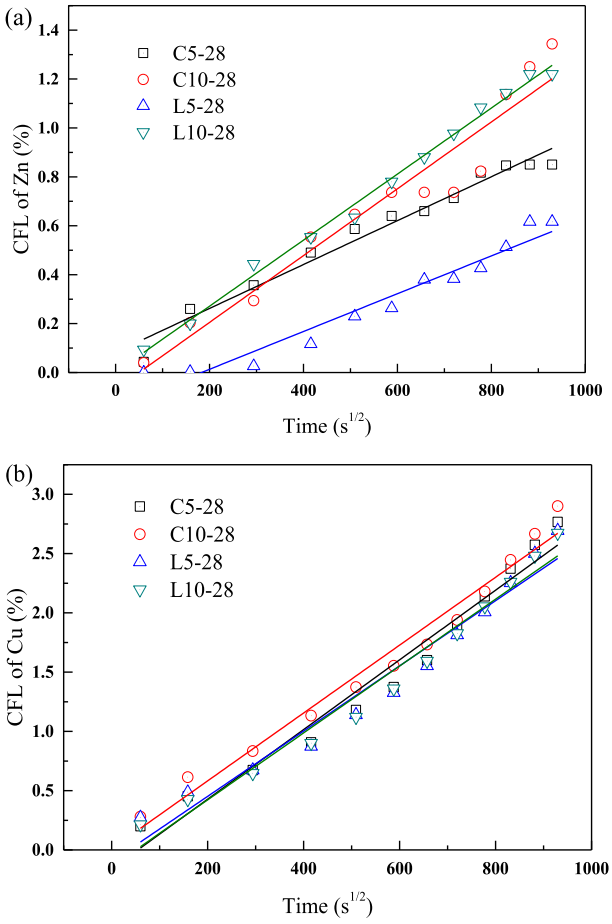

Fig. 10. CFL of (a) Zn and (b) Cu in the 28-d mortar samples.

the required minimum compressive strength of 4.14 MPa for non-load bearing uses (Wang et al., 2015b). However, considering the economic and environmental aspects, application of lime-ISSA treated sediments as filling materials was more cost-effective and promising.

In Fig. 5b, the failure strain of all the mortar samples increased in general with increasing curing time and binder contents except for C10 (it is very likely due to inhomogeneity of the specimens). Therefore, the failure strain of these samples showed a consistent trend with that of the UCS. That is to say, the S/S treated sediment is a ductile material and the ductility of sediment can be improved during the S/S process. The failure strains of all the S/S treated sediments ranged from 3% to 7%, indicating a good ductility.

The deformation modulus E_{50} throughout the whole curing period and its relationship with stress are shown in Fig. 6a and b, respectively. All the samples had the highest E_{50} at 28 d except L10, whose UCS increased significantly from 28 d to 90 d. Due to its high strength, the C10 sample had the highest E_{50}, implicating its highest resistance capacity to deformation (Lee et al., 2005). In addition, E_{50} increased with the binder content, and the cement samples showed a higher value than the lime samples under the same binder dosage.

In Fig. 6b, the change of E_{50} is consistent with the strength development and a linear correlation fitting is found to be $y = 12.56x + 12.36$ ($R^2 = 0.953$), which is consistent with a previous research (Cai et al., 2015).

Fig. 7 illustrates the durability test results expressed as strength before and after 30 d of water soaking. The mortar samples prepared with lower binder contents (C5 and L5) experienced a slight drop in strength after further soaking for 30 d, whereas the strengths of C10 and L10 increased noticeably after water soaking. For the samples prepared with lower binder contents, the content of $Ca(OH)_2$ was too low to react with ISSA which only possessed a moderate pozzolanic activity. The relatively small amount of hydration products could not hold the samples together when they were soaked in water. Whereas further water soaking provided more available water for the hydration processes of C10 and L10, the ISSA might be activated by the higher $Ca(OH)_2$ content (Zhou et al., 2019), which led to an improvement of strength. Based on the durability test results, the lime-ISSA treated sediment (i.e. L10) would be more suitable for production of the low strength filling materials.

3.4. Environmental impacts

As the Zn and Cu concentrations in the raw sediment and ISSA were relatively high, they were major concerns for evaluating the

Table 3
De values of Cu and Zn of 28-d mortar samples.

Sample	*De* (m^2/s)	
	Cu	Zn
C5-28	4.71×10^{-14}	4.39×10^{-15}
C10-28	4.46×10^{-14}	1.02×10^{-14}
L5-28	4.12×10^{-14}	3.25×10^{-15}
L10-28	4.33×10^{-14}	9.93×10^{-15}

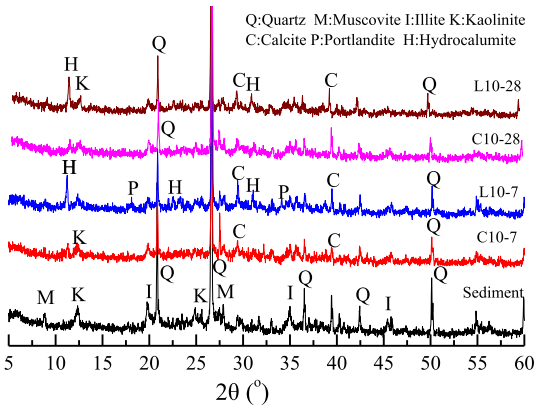

Fig. 11. XRD spectra of raw sediment, C10 and L10 at 7 d and 28 d (M: muscovite; K: Kaolinite; Z: zeolite; P: portlandite; C: calcite; H: hydrocalumite; Q: quartz; I: Illite).

environmental impacts of the mortar samples. Fig. 8 shows the leachability of Zn and Cu of the raw sediment and the treated sediment at 7 d and 28 d. It is known that the ISSA used in this study was considered as a non-hazardous material (Li and Poon, 2017). As shown in Fig. 8, the leachate concentrations of Zn (1.98 mg/L) and Cu (0.12 mg/L)of the raw sediment were within the TCLP limits of heavy metals based on USEPA (2018) universal treatment standard. Nevertheless, it is still necessary to study the potential environmental risks of the treated sediment under extreme conditions. After applying the ISSA alone, the leachate concentration of both Zn and Cu increased as these two metals were also presented in the ISSA; but they decreased with addition of OPC and lime, especially for lime mostly due to the higher pH value of lime-treated samples. The Zn and Cu concentrations were significantly lower than the UTS limit in the C10 and L10 samples. Our previous study also confirmed that the pollutants could be physically encapsulated and/or chemically fixed by the hydration products (Li et al., 2017c). For most samples, the leaching concentration of Zn decreased with time but that of Cu increased. It can be attributed to the complex variations of scenario in the S/S samples, such as pH value, redox and chemical compositions. Based on the TCLP results, the treated sediment mortars were applicable without environmental risks, especially for the lime-based samples (Cote et al., 1987; Tang et al., 2019).

The semi-dynamic leaching test results of the monolithic mortar samples at 28 d are shown in Fig. 9, indicating the long-term leaching behaviors of the heavy metals. Very low concentrations of Zn and Cu were detected from the 28-d mortar samples due to

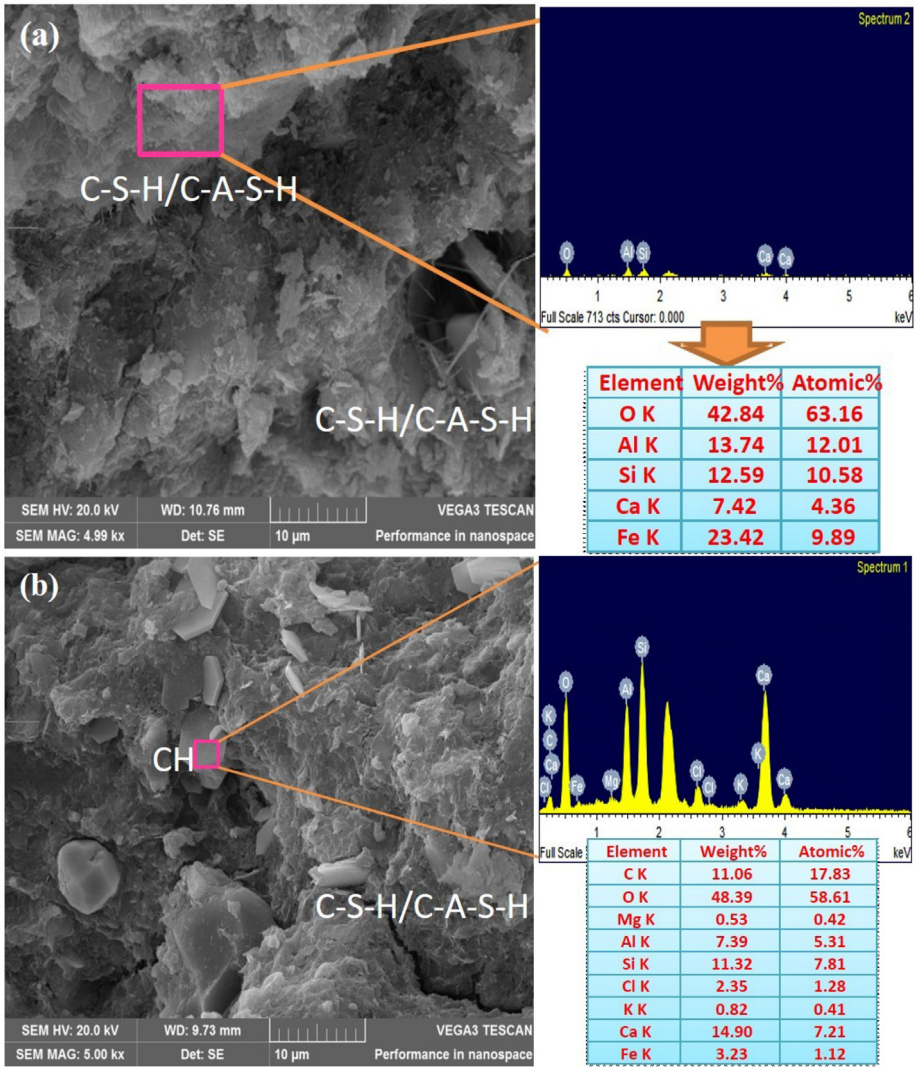

Fig. 12. SEM images with EDX results of (a) C10 and (b) L10 at 28 d.

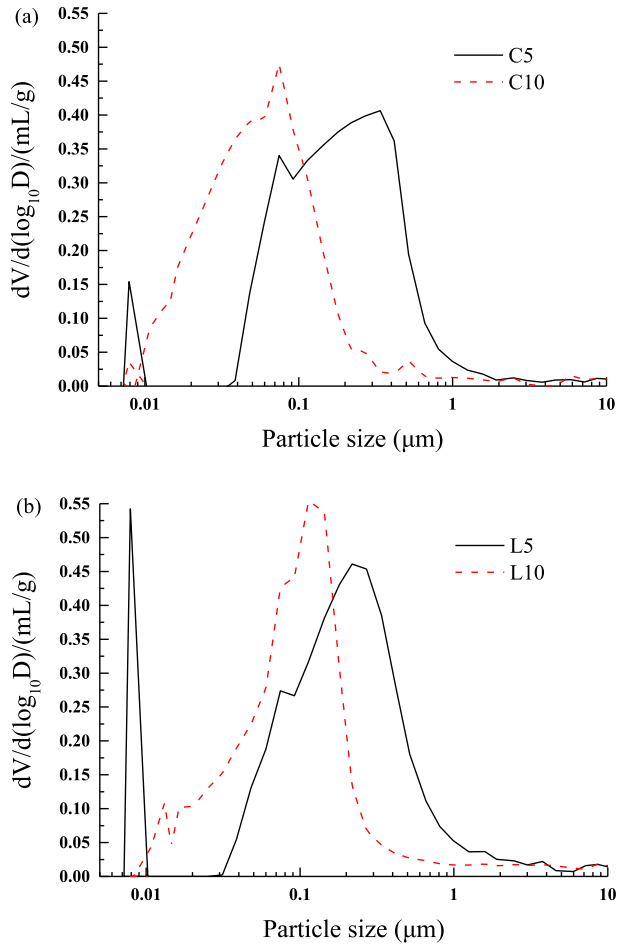

Fig. 13. Pore size distribution of (a) C5, C10 and (b) L5, L10 at 28 d.

encapsulation or precipitation in the treated sediment. The concentrations of Zn and Cu ranged from 0.001 mg/L to 0.094 mg/L, and 0.027 mg/L to 0.05 mg/L, respectively. Also, the cumulative leached amounts of Zn and Cu were far below the limit value in the Dutch legislation-the soil quality decree (SQD), which demonstrates the non-hazardous nature of the treated sediment to the environment (Soil Quality Decree, 2013).

Fig. 10 presents the CFL of Zn and Cu against $t^{1/2}$of the mortar samples at 28 d. Only small amounts of Zn and Cu were leached during the test. In the first day, only less than 0.2% of Zn and 0.5% of Cu were leached out from all the S/S samples. The linear plots suggested that Zn and Cu leaching was mainly controlled by diffusion in the whole process. The calculated *De* values of Zn and Cu are listed in Table 3. All the values varied from 9.93×10^{-15} m^2/s to 1.02×10^{-14} m^2/s which were smaller than10^{-13} m^2/s, indicating that the treated sediment had low leaching risks and were feasible to be used as filling materials (Li et al., 2017c).

3.5. Microscopic analysis

3.5.1. XRD results

The XRD spectra of the raw sediment, C10 and L10 at the curing ages of 7 d and 28 d are shown in Fig. 11. The crystalline phases of the raw sediment mainly consisted of muscovite, kaolinite, illite and quartz. After treated by OPC/lime-ISSA, calcite was detected in C10 and L10 and it could be attributed to the carbonation of $Ca(OH)_2$ during curing process. As a consequence, hydrocalumite was only presented in L10 and minor portlandite only appeared in L10 at 7 d due to consumption by ISSA, carbonation and its limited amount especially for C10. The formation of hydrocalumite that can contribute to the strength development of the sediment mortar might be due to the reaction between $Ca(OH)_2$ and the partial soluble Al presented in the raw sediment. The XRD patterns of C10 and L10 did not show significant differences, but a slightly higher calcite peak in C10 and L10 cured for 28 d was observed compared with the samples at 7 d. The calcite might also facilitate strength development of the mortars with increase in curing time. In addition, there were no Zn- and Cu-containing crystalline products detected after the S/S process, which might be: (a) the contents of related phases were too low to be detected by XRD, and (b) the chemical reactions of Zn and Cu species were weak (Wang et al., 2018).

3.5.2. SEM-EDX results

Fig. 12 shows the SEM micrographs with EDX analysis of C10 and L10 after 28 d of curing. In Fig. 12a, a large amount of amorphous C–S–H/C-A-S-H gels mainly produced from OPC hydration were observed and formed on the surface of sediment in C10 at 28 d. The EDX results indicated the presence of Fe which might be originally from ISSA. As shown in Fig. 12b, some plate-like crystals known to be $Ca(OH)_2$ (CH) were visible (although some were carbonated by CO_2) and intersected with the gels in L10; but there was a less amount of gel-like phases than C10 due to moderate pozzolanic reactions of CH with ISSA. These findings confirmed that ISSA and sediment possibly reacted with $Ca(OH)_2$ to form hydration products. The sources of Si and Al were provided by ISSA and sediment particles, and then they reacted with lime to form C-A-S-H gel which filled the space, producing a relatively dense microstructure to enhance the strength development (Hwang et al., 2014). In addition, the formed C-A-S-H gels could also provide active sites for immobilization of heavy metals such as Zn and Cu via adsorption and precipitation (Wang et al., 2018; Zha et al., 2019).

3.5.3. MIP results

The pore size distributions of the mortar samples at 28 d measured by MIP are plotted in Fig. 13. It is obvious that the peak of the major pore size shifted to the left when using higher binder content (i.e. C10 and L10). Most of the pore size in the range of 0.1–1 μm (intra-aggregate pores) shifted to 0.01–1 μm (inter-aggregate pores) (Hattab et al., 2013). This means that more $Ca(OH)_2$ and hydration products such as C–S–H gel were formed during the hydration reaction to fill the space between the sediment particles. Additionally, with a higher binder and $Ca(OH)_2$ contents, more secondary hydration products were formed and filled the larger pores due to the pozzolanic reactions with ISSA.

3.5.4. TGA and DTG results

The thermogravimetric analysis (TGA) test was performed on the raw sediment, sediment-ISSA mixture and mortar samples at 28 d from 50 °C to 1000 °C. The mass loss and associated derivative thermogravimetry (DTG) results are shown in Fig. 14. The peak of DTG curves in a range of (100–200) °C corresponded to the dehydroxylation of C–S–H gel (Scrivener et al., 2017). The peak of DTG value between 380 °C and 450 °C was due to dehydroxylation of portlandite (Scrivener et al., 2017) and it can be seen from Fig. 14a that the peak at (400–500) °C was caused by the decomposition of organic matter in the raw sediment (Wang et al., 2015b). The decomposition of $CaCO_3$ occurred around (500–800) °C (Scrivener et al., 2017). Table 4 summarized the mass loss at different temperature ranges of all the samples. In the untreated sediment and SD samples, the mass loss at (380–450) °C was mainly affected by the presence of organics rather than $Ca(OH)_2$. There was a small amount of $CaCO_3$ originally presented in the SED and SD. After

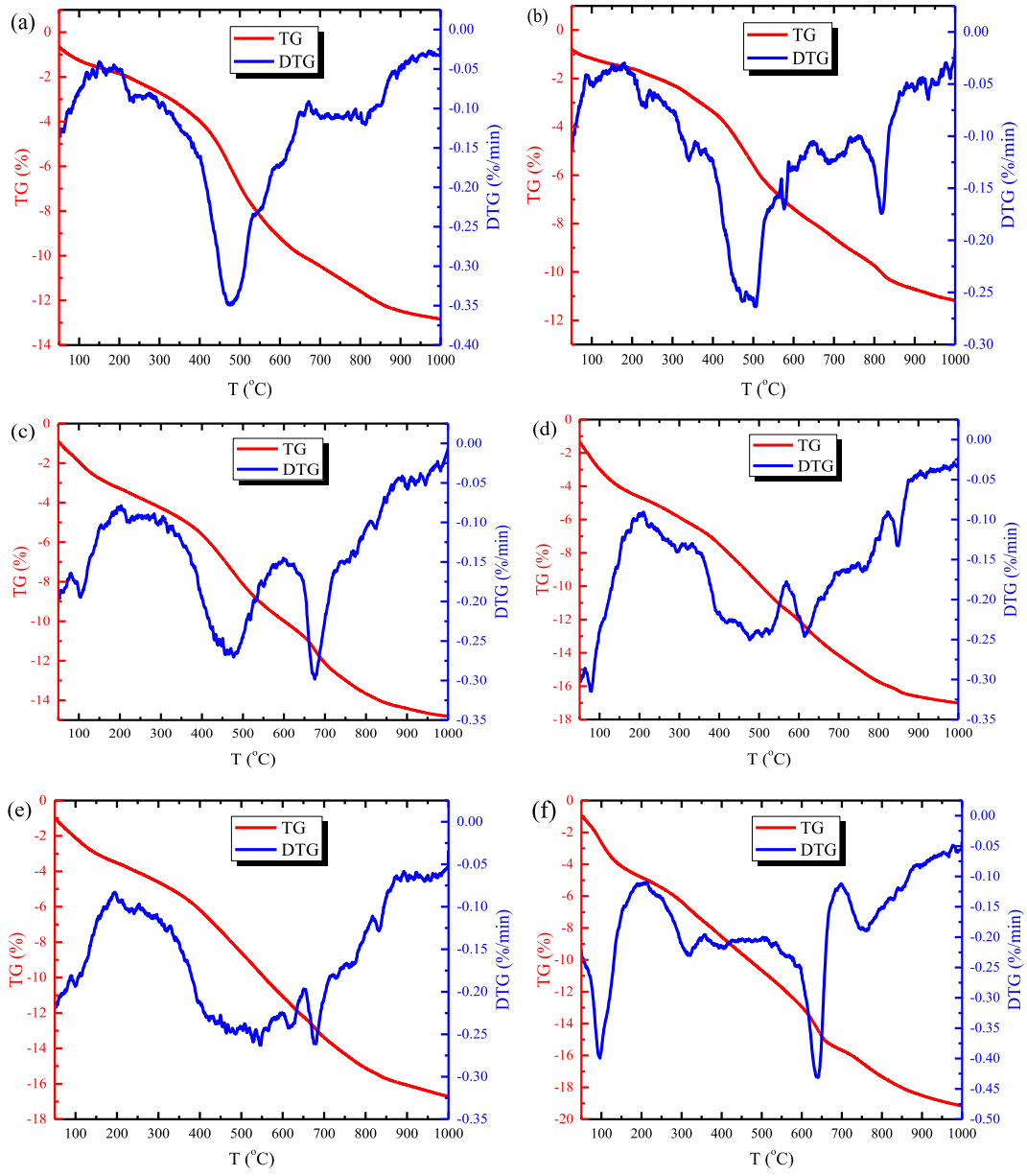

Fig. 14. TG and DTG curves of (a) SED, (b) SD, (c) C5, (d) C10, (e) L5 and (f) L10 samples at 28 d.

Table 4
Mass loss of SED, SD and mortar samples at 28 d of curing.

Temperature (°C)	Mass loss (%)					
	SED	SD	C5	C10	L5	L10
100–200	0.599	0.423	1.353	1.651	1.418	2.164
380–450	1.483	1.161	1.545	1.579	1.577	1.518
500–800	5.617	5.147	6.281	6.769	7.486	7.852

addition of OPC, the mass loss due to the decomposition of the hydration products increased and C10 showed a higher mass loss than C5, suggesting that a higher amount of hydration products was formed in C10. The results were consistent with the MIP results and strength development. The content of $CaCO_3$ was also larger in C10 due to carbonation of $Ca(OH)_2$. For the lime-treated sediment, a comparable $Ca(OH)_2$ content was found in the OPC-treated sediment, the amount of which was greater in L5 than that in L10. This indicates that a significant amount of $Ca(OH)_2$ was consumed by ISSA/sediment as well as carbonated to $CaCO_3$, as the mass loss at (100–200) °C and (500–800) °C both increased from L5 to L10. The lime-treated sediment generally had a higher amount of $CaCO_3$ than the OPC-treated one, as the former had a lower strength and a larger porosity which was susceptible to carbonation. Also, lime was much easier to react with CO_2 (Zhou et al., 2019).

4. Conclusions

This paper reported a study on the S/S treatment of CMS with high water content using a combination of high content of ISSA and OPC/lime binders. The strength, engineering properties, leaching potential and microstructural changes of the treated sediment samples were discussed. It was found that the treated sediment had an improved strength, resistance to deformation, durability, and reduced workability especially for the samples treated with elapsed lime. The L10 sample reached 1.6 MPa after curing for 28 d, which satisfied the requirement for use as on-site filling materials. The

leaching results from TCLP and semi-dynamic leaching test suggested a low environmental risk of the treated sediment and revealed possible effectiveness of this S/S treatment system for Cu and Zn immobilization. The hydration products such as C–S–H, C-A-S-H gel and/or hydrocalumite, which produced from OPC hydration and pozzolanic reactions with ISSA, were found in both OPC- and lime-treated sediments. The amount of hydration products increased with increased binder contents and hence the porosity measured by MIP decreased. Treating the contaminated sediment using high content of ISSA and lime (the dosage may depend on the application case) not only provided a sustainable recycling route for waste materials to be used as construction materials, but also lowered the costs and environmental impacts.

Declaration of competing interest

The authors declare that they have no known competing financial interests or personal relationships that could have appeared to influence the work reported in this paper.

Acknowledgments

The authors would like to thank the financial support of National Natural Science Foundation of China (Grant Nos. 51861165104 and 51625903), and National Key Research and Development Project (Grant No. 2019YFC1804002).

References

American Concrete Institute ACI 229R-99, 1999. Controlled Low Strength Materials. ACI, Farmington Hills, MI, USA.
STM C109/C109M-08, 2008. Standard Test Method for Compressive Strength of Hydraulic Cement Mortars. ASTM International, West Conshohocken, PA, USA.
STM C1437-15, 2015. Standard Test Method for Flow of Hydraulic Cement Mortar. ASTM International, West Conshohocken, PA, USA.
BS EN 12390-3, 2009. Testing Hardened Concrete. Part 3: Compressive Strength of Test Specimens. British Standards Institution, London, UK.
Cai, G.H., Liu, S.Y., Du, Y.J., Zhang, D.W., Zheng, X., 2015. Strength and deformation characteristics of carbonated reactive magnesia treated silt soil. J. Cent. S. Univ. 22, 1859–1868.
Chen, L., Lin, D.F., 2009. Stabilization treatment of soft subgrade soil by sewage sludge ash and cement. J. Hazard Mater. 162 (1), 321–327.
Chen, Z., Poon, C.S., 2017. Comparative studies on the effects of sewage sludge ash and fly ash on cement hydration and properties of cement mortars. Construct. Build. Mater. 154, 791–803.
Chen, Z., Li, J.S., Poon, C.S., 2018. Combined use of sewage sludge ash and recycled glass cullet for the production of concrete blocks. J. Clean. Prod. 171, 1447–1459.
Cote, P.L., Constable, T.W., Moreira, A., 1987. An evaluation of cement-based waste forms using the results of approximately two years of dynamic leaching. Nucl. Chem. Waste Manag. 7 (2), 129–139.
Fang, L., Li, J.S., Guo, M.Z., Cheeseman, C.R., Tsang, D.C., Donatello, S., et al., 2018. Phosphorus recovery and leaching of trace elements from incinerated sewage sludge ash (ISSA). Chemosphere 193, 278–287.
Garcia-Lodeiro, I., Fernández-Jiménez, A., Palomo, A., 2013. Variation in hybrid cements over time. Alkaline activation of fly ash–Portland cement blends. Cement Concr. Res. 52, 112–122.
HK E TWB Management of dredged/excavated sediment, 2002. Technical Circular (Works) No. 34/2002. ETWB(W) 209/32/96. Hong Kong: Environment. Transport and Works Bureau.
Hattab, M., Hammad, T., Fleureau, J.M., Hicher, P.Y., 2013. Behaviour of a sensitive marine sediment: microstructural investigation. Geotechnique 63 (1), 71–84.
Hwang, K.Y., Seo, J.Y., Phan, H.Q., Ahn, J.Y., Hwang, I., 2014. MgO-based binder for treating contaminated sediments: characteristics of metal stabilization and mineral carbonation. Clean 42 (3), 355–363.
Izaguirre, A., Lanas, J., Álvarez, J.I., 2010. Behaviour of a starch as a viscosity modifier for aerial lime-based mortars. Carbohydr. Polym. 80 (1), 222–228.
Lee, F.H., Lee, Y., Chew, S.H., Yong, K.Y., 2005. Strength and modulus of marine clay-cement mixes. J. Geotech. Geoenviron. Eng. 131 (2), 178–186.
Li, J.S., Poon, C.S., 2017. Innovative solidification/stabilization of lead contaminated soil using incineration sewage sludge ash. Chemosphere 173, 143–152.
Li, J.S., Guo, M.Z., Xue, Q., Poon, C.S., 2017a. Recycling of incinerated sewage sludge ash and cathode ray tube funnel glass in cement mortars. J. Clean. Prod. 152, 142–149.
Li, J.S., Xue, Q., Fang, L., Poon, C.S., 2017b. Characteristics and metal leachability of incinerated sewage sludge ash and air pollution control residues from Hong Kong evaluated by different methods. Waste Manag. 64, 161–170.
Li, J.S., Wang, L., Tsang, D.C., Beiyuan, J., Poon, C.S., 2017c. Dynamic leaching behavior of geogenic as in soils after cement-based stabilization/solidification. Environ. Sci. Pollut. Res. 24 (36), 27822–27832.
Li, J.S., Zhou, Y.F., Wang, Q.M., Xue, Q., Poon, C.S., 2019. Development of a novel binder using lime and incinerated sewage sludge ash to stabilize and solidify contaminated marine sediments with high water content as a fill material. J. Mater. Civ. Eng. 31 (10), 04019245.
Lirer, S., Liguori, B., Capasso, I., Flora, A., Caputo, D., 2017. Mechanical and chemical properties of composite materials made of dredged sediments in a fly-ash based geopolymer. J. Environ. Manag. 191, 1–7.
Scrivener, K., Snellings, R., Lothenbach, B., 2017. A Practical Guide to Microstructural Analysis of Cementitious Materials. CRC Press, Taylor & Francis Group, Boca Raton. https://doi.org/10.1201/b19074.
Senff, L., Hotza, D., Repette, W.L., Ferreira, V.M., Labrincha, J.A., 2010. Rheological characterisation of cement pastes with nanosilica, silica fume and superplasticiser additions. Adv. Appl. Ceram. 109 (4), 213–218.
Soil Quality Decree Regeling bodemkwaliteit, VROM, den haag, 2013. Ruimteen Milieu. Ministerie van Volk shuisvesting, Ruimtelijke Ordeling en Milieubeheer (In Dutch).
Tang, Q., Shi, P., Yuan, Z., Shi, S., Xu, X., Katsumi, T., 2019. Potential of zero-valent iron in remediation of Cd (II) contaminated soil: from laboratory experiment, mechanism study to field application. Soils Found. 59 (6), 2099–2109.
US EPA Method 1311, 1992. Toxicity Characteristic Leaching Procedure, Part of Test Methods for Evaluating Solid Waste, Physical/chemical Methods. Environmental Protection Agency, Washington, D.C., USA.
US EPA Universal Treatment Standard (US 40 CFR 268.48), 2018. Environmental Protection Agency, Washington, D.C., USA.
Wang, D., Abriak, N., Zentar, R., 2017. Dredged marine sediments used as novel supply of filling materials for road construction. Mar. Georesour. Geotechnol. 35 (4), 472–480.
Wang, D., Zentar, R., Abriak, N.E., Di, S., 2018. Long-term mechanical performance of marine sediments solidified with cement, lime, and fly ash. Mar. Georesour. Geotechnol. 36 (1), 123–130.
Wang, L., Tsang, D.C., Poon, C.S., 2015a. Green remediation and recycling of contaminated sediment by waste-incorporated stabilization/solidification. Chemosphere 122, 257–264.
Wang, L., Kwok, J.S., Tsang, D.C., Poon, C.S., 2015b. Mixture design and treatment methods for recycling contaminated sediment. J. Hazard Mater. 283, 623–632.
Wang, L., Yu, K.Q., Li, J.S., Tsang, D.C., Poon, C.S., Yoo, J.C., et al., 2018. Low-carbon and low-alkalinity stabilization/solidification of high-Pb contaminated soil. Chem. Eng. J. 351, 418–427.
Wang, Y.S., Dai, J.G., Wang, L., Tsang, D.C., Poon, C.S., 2018. Influence of lead on stabilization/solidification by ordinary Portland cement and magnesium phosphate cement. Chemosphere 190, 90–96.
Zentar, R., Miraoui, M., Abriak, N.E., Benzerzour, M., 2011. Natural dewatering of marine dredged sediments. Dry. Technol. 29 (14), 1705–1713.
Zentar, R., Wang, D., Abria, N.E., Benzerzour, M., Chen, W., 2012. Utilization of siliceous–aluminous fly ash and cement for solidification of marine sediments. Construct. Build. Mater. 35, 856–863.
Zha, F., Ji, C., Xu, L., Kang, B., Yang, C., Chu, C., 2019. Assessment of strength and leaching characteristics of heavy metal–contaminated soils solidified/stabilized by cement/fly ash. Environ. Sci. Pollut. Control Ser. 26 (29), 30206–30219.
Zhou, Y.F., Li, J.S., Lu, J.X., Cheeseman, C., Poon, C.S., 2020. Recycling incinerated sewage sludge ash (ISSA) as a cementitious binder by lime activation. J. Clean. Prod. 244, 118856.

Prof. Jiang-Shan Li is professor of geotechnical engineering at Institute of Rock and Soil Mechanics, Chinese Academy of Sciences, the director of IRSM-CAS/HKPolyU Joint Laboratory on Solid Waste Science, and Hong Kong scholar. His research areas include geo-environmental engineering and solid waste recycling. He is principal investigator (PI) of one project sponsored by National Natural Science Foundation of China (NSFC) and sub-PI of National Key R&D Program of China. Prof. Li is a member of Youth Working Committee of Soil Mechanics and Geotechnical Engineering Branch in Chinese Civil Engineering Society, Tailing and Mine Wastes Committee of International Society for Soil Mechanics and Geotechnical Engineering, Youth Working Committee of Environmental Geotechnical Engineering Branch in Chinese Society for Rock Mechanics and Engineering, and journal editor of *Environmental Geotechnics*. Prof. Li authored over 80 journal papers, among which 69 papers were published in international journals and indexed by SCI database.